Exit time of colloidal particles from falling drops

Nishanth Murugan and Anubhab Roy*
Department of Applied Mechanics, Indian Institute of Technology Madras, Chennai 600036, India

(Received 17 June 2025; accepted 26 November 2025; published 17 December 2025)

This work investigates the influence of convective transport within a sedimenting drop on the exit time of a colloidal particle. Using Brownian dynamics simulations, we compute exit times for particles originating from various locations inside the drop over a range of Péclet numbers (Pe). The Péclet number quantifies the balance between the convective transport, caused by the Hadamard-Rybczynski flow field within a sedimenting drop, and the thermal fluctuations in the system. Additionally, we model the exit time as a first-passage process governed by the backward Kolmogorov equation, solving it asymptotically for $\mathrm{Pe} \ll 1$ and $\mathrm{Pe} \gg 1$, as well as numerically, to determine the mean exit time as a function of Pe.

DOI: 10.1103/h8sk-8kp7

I. INTRODUCTION

Particle-laden droplets are prevalent in numerous natural and environmental systems, playing a crucial role in phenomena ranging from raindrop formation in clouds to pathogen-laden aerosol transport. Understanding fluid transport and mixing within such droplets is essential, as it directly influences their physical and chemical dynamics. Traditionally, particle transport in these systems has been characterized using an effective diffusivity or mean-squared displacement. In this work, we adopt an alternative approach by leveraging the concept of first-passage exit time [1]—the time it takes for a particle to leave the droplet—to gain deeper insights into its transport behavior. This perspective is particularly relevant for studying aerosol-mediated pathogen dispersion, where droplet evaporation and gravitational settling affect how long infectious agents remain airborne. Additionally, our findings have broader implications for understanding droplet coalescence in condensing cloud droplets, as well as transport processes in environmental flows, such as volcanic ash dispersion and pollutant dynamics in atmospheric aerosols.

Colloidal particles suspended in cloud droplets play a crucial role in cloud microphysics by influencing droplet stability, growth, and phase transitions [2]. These particles, which include insoluble mineral dust, soot, biological aerosols, and organic matter, can act as cloud condensation nuclei or ice nucleating particles, affecting cloud droplet formation and ice crystal development. Their presence alters the optical and radiative properties of clouds, impacting cloud albedo and lifetime. Additionally, colloidal particles can modify the chemical composition of cloud water, catalyzing heterogeneous reactions that influence atmospheric chemistry and precipitation processes. Understanding their behavior is essential for improving predictions of cloud dynamics, precipitation efficiency, and climate feedback mechanisms.

The study of heat and mass transport from drops has been extensively explored, particularly in the regime of strong convection effects ($\mathrm{Pe} \gg 1$), where the Péclet number (Pe) characterizes the relative dominance of convection over diffusion. Early work by Kronig and Brink [3] focused on estimating heat transport from a falling drop by calculating the Nusselt number in the asymptotic limits of weak and strong convection over long timescales. This was later refined by Oliver and Souccar [4], who employed improved numerical methods to capture heat transfer at finite times, revealing the presence of a boundary layer near the drop surface where diffusion and convection effects become comparable. In a related effort, Yu-Fang and Acrivos [5] computed the average Nusselt number in a doubly connected convection-dominated flow field with closed streamlines, analyzing various Reynolds number (Re) regimes. Their results demonstrated that for both $\mathrm{Re} \ll 1$ (Stokes regime) and $\mathrm{Re} \gg 1$ (a core of constant vorticity with a shear layer at the boundary), heat transport remains independent of Pe and Re, with variations emerging only at finite Re due to evolving streamline patterns driven by the interplay of viscous and inertial forces. In the context of passive scalar transport, Lingevitch and Bernoff [6] studied advection in a Lamb dipole flow, deriving an averaged diffusion equation in the $\mathrm{Pe} \gg 1$ limit using homogenization theory and a coordinate transformation along flow streamlines. Their findings also highlighted the formation of a boundary layer of width $\mathrm{Pe}^{-1/2}$ along both the drop boundary and the centerline, where the passive scalar is rapidly expelled. A similar framework applies to particle transport in a rising hot buoyant fluid parcel (a thermal), where Griffiths [7] examined the high-Rayleigh-number ($\mathrm{Ra} \gg 1$) regime and identified a thin boundary layer responsible for fluid entrainment from outside the thermal, thereby controlling both the rate of mass exchange across the interface and the residence time of suspended particles within the thermal. Following the approach of Lingevitch and Bernoff [6], he modeled the exterior flow as potential flow and the interior as a Hill's spherical vortex, incorporating a kinematic description of a highly viscous expanding thermal, akin to the work of Turner [8]. These studies collectively underscore the crucial role of boundary layers in governing transport processes within convective flows.

Beyond the role of steady advection, Lagrangian chaos has been shown to significantly enhance transport in various systems [9] and is particularly relevant to the mixing and

*Contact author: anubhab@iitm.ac.in

stirring of particle-laden fluids. In the context of heat and mass transfer from liquid drops, this has led to substantial interest in the generation and characterization of chaotic flow fields. Bajer and Moffatt [10] first mathematically constructed a three-dimensional quadratic Stokes flow field within a droplet, demonstrating the existence of chaotic streamlines in the noninertial regime. Building on this, Stone *et al.* [11] linked these chaotic streamlines to a physically realizable system—a non-neutrally buoyant droplet in a linear shear flow with background vorticity—and characterized the transport using Poincaré sections. Their work further revealed that the extent of chaotic behavior depended on the angle between the principal strain axes and the vorticity vector, as well as the relative magnitude of the vorticity tensor compared to the strain rate tensor. Bryden and Brenner [12] extended this study by incorporating the translation of a non-neutrally buoyant drop relative to the bulk fluid, demonstrating significant alterations in the Poincaré sections. Later, Kroujiline and Stone [13] explored chaotic trajectories in the quadratic flow field of a translating drop within a bulk fluid with background vorticity, deriving the corresponding Poincaré sections. In a different setting, Christov and Homsy [14] investigated how the presence of an axial electric field modifies heat and mass transport from falling drops, showing that increasing field strength transforms the internal flow from the Hadamard-Rybczynski profile to an antisymmetric Taylor flow. More recently, Krishnamurthy and Subramanian [15] examined heat and mass transport from a neutrally buoyant droplet in planar linear and three-dimensional extensional flows, focusing on the small Reynolds number ($\mathrm{Re} \ll 1$) and large Péclet number ($\mathrm{Pe} \gg 1$) limit. By shifting to a nonorthogonal coordinate system aligned with the flow streamlines, they derived a similarity solution for the advection-diffusion equation governing heat transport, particularly within the open-streamline regime. These studies collectively underscore the crucial role of chaotic advection in enhancing transport processes in droplet-laden flows. The aforementioned studies have primarily characterized heat and mass transport from liquid drops by analyzing the long-time behavior of particle transport across various settings. However, a significant challenge in understanding transport in chaotic flows lies in estimating their finite-time behavior, which is complicated by the nonintegrable nature of the underlying flow fields. In this context, the concept of exit time—framing particle transport as a first-passage process [1]—offers a particularly useful approach. Batchelor and Nitsche [16] investigated this idea in the context of non-neutrally buoyant drops in gas-fluidized beds, defining an exit-time metric (T_{90}) as the time required for 90% of the particles to exit the drop. Their study sought to explain the formation of clear bubbles devoid of particles in gas-fluidized beds—an observation contrasting with liquid-fluidized beds—ultimately attributing the difference to the weaker particle expulsion mechanism in the latter due to the higher viscosity and density of the surrounding fluid. More broadly, following the framework of Redner [1], exit time can be rigorously formulated as a first-passage process, leading to a backward Kolmogorov equation governing its dynamics [17]. In a related study, Marcotte *et al.* [18] tackled the inverse problem, optimizing the time-dependent flow field within a drop to maximize heat transfer through its boundaries—an approach conceptually similar to modeling the exit of colloidal particles from confined domains. Building upon these insights, the objective of this paper is to compute the finite-time exit of a colloidal particle from a falling drop and estimate its mean exit time, thereby advancing our understanding of transport in convective and chaotic droplet flows.

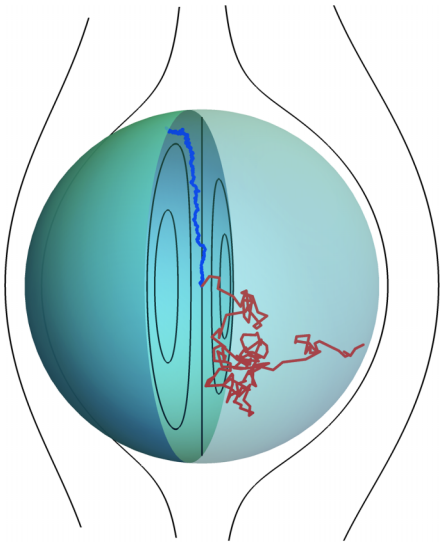

FIG. 1. Trajectory of a Brownian particle starting at the drop center (0,0,0) for $\mathrm{Pe} = 1000$ (blue line) and $\mathrm{Pe} = 0.1$ (red line) depicting the effects of convective transport inside a sedimenting drop. The black lines depict the streamlines associated with the Hadamard-Rybczynski flow field in a comoving reference frame.

The flow field inside a falling drop, as described by the Hadamard-Rybczynski solution, consists of closed streamlines. While convection influences particle motion within the drop, the eventual escape of a particle is facilitated solely by thermal fluctuations that enable diffusion across these closed flow paths. A nondimensional Péclet number, $\mathrm{Pe} = \bar{U}R/(2D(1+\lambda))$, where $\lambda = \widehat{\mu}/\mu$ with $\widehat{\mu}$ and μ being the viscosities pertaining to the drop and the ambient medium where the drop is present, $\bar{U}$ is the terminal velocity attained by the freely falling drop, and D is the diffusivity characterizing the thermal fluctuations in the system. The particle trajectories associated with the exit of a colloidal particle in the presence and absence of convective effects are displayed in Fig. 1. In the absence of any thermal fluctuations in the system, the particle transport can be described by a Hamiltonian system as shown in Kroujiline and Stone [13]. The current work can thus be thought of as a Hamiltonian system that is perturbed by a stochastic noise. The role of convective transport is more prominently showcased in Fig. 2, wherein a line of 2×10^5 particles is allowed to evolve for $\mathrm{Pe} = 1000$. Figures 2(a)–2(c) depict the fine structure associated with the convective transport at earlier times, whereas at later times, as shown in Figs. 2(d)–2(f), the diffusive transport serves to disperse the structure formed by the convective transport.

Everyday actions such as breathing, speaking, coughing, or sneezing by an infected individual generate pathogen-laden droplets, which serve as vehicles for airborne disease transmission. These droplets, carrying viruses or bacteria, play a crucial role in spreading infections to a larger population. The

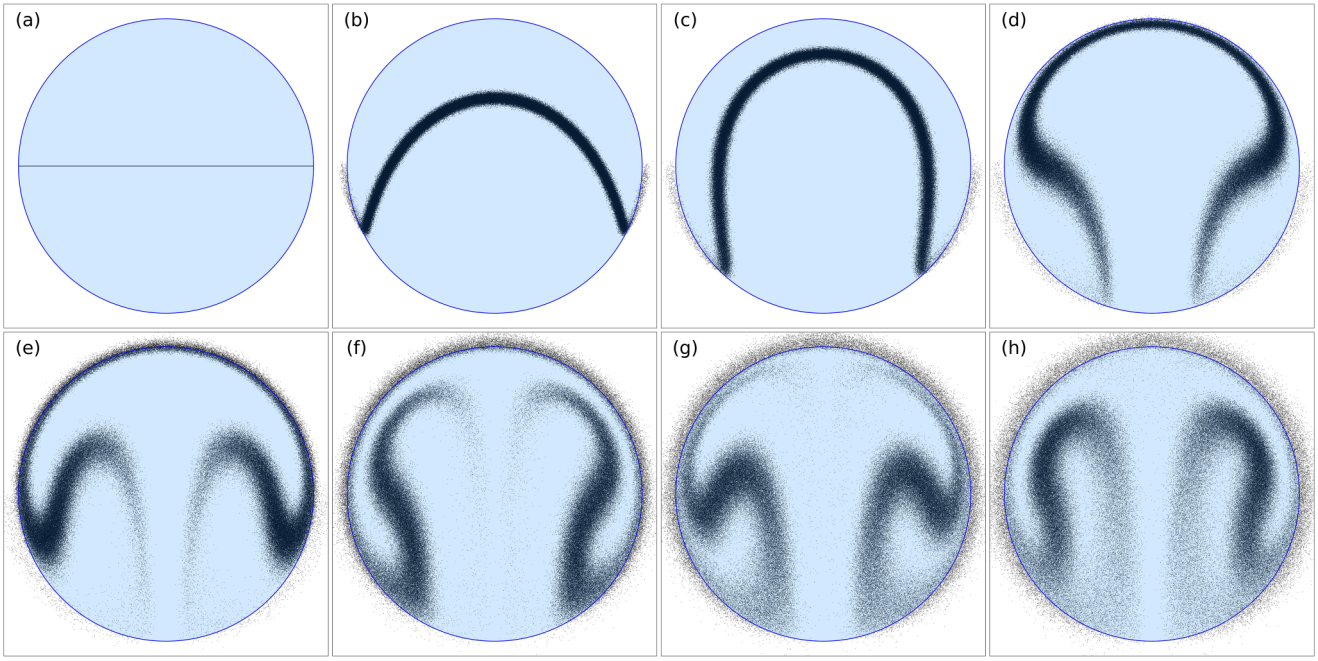

FIG. 2. The transport of a line comprising 2×10^5 particles inside a sedimenting drop for Pe = 1000 at times (a) $t = 0$, (b) $t = 0.5$, (c) $t = 1$, (d) $t = 2$, (e) $t = 3$, (f) $t = 4$, (g) $t = 5$, and (h) $t = 6$ where t has been nondimensionalized using a convective timescale ($R/\bar{U}$).

fluid dynamics of transport and mixing fundamentally dictate the behavior of pathogens within exhaled droplets, with the droplet radius being a key factor in determining the governing physical mechanisms. The size distribution of these droplets is highly dependent on the mode of generation—whether through a cough, sneeze, or speech—each producing a distinct spectrum of droplet sizes [19]. A critical aspect of disease transmission is the concept of residence time, which refers to the duration that these pathogen-laden droplets remain suspended in the air before settling due to gravity. If the exit time of a pathogen from the droplet is shorter than the droplet's residence time, the pathogen can escape into the surrounding air and remain suspended, thereby substantially elevating the risk of airborne transmission. Understanding these processes is essential for predicting and mitigating the spread of airborne diseases.

In this paper, we examine the influence of convective transport on the exit of colloidal-sized particles from sedimenting drops. In Sec. II, we employ Brownian dynamics simulations to estimate the exit time. However, due to the computational complexity of these simulations, they are impractical for obtaining a mean exit time across different Péclet numbers (Pe). To address this limitation, in Sec. III, we formulate the exit-time problem stochastically as a first-passage process governed by a backward Kolmogorov equation, drawing on the work of Redner [1], Thiffeault [17], Souccar and Oliver [20], and Kronig and Brink [3]. Section III A explores the small-Pe (Pe $\ll 1$) asymptotics using perturbation expansions, while Sec. III B extends the analysis to the large-Pe (Pe $\gg 1$) regime by transforming the problem into a coordinate system aligned with the flow streamlines, following the approach of Kronig and Brink [3].

II. BROWNIAN DYNAMICS

The velocity field experienced by a colloidal particle due to the thermal fluctuations of the medium where it is present is given by $d\boldsymbol{x}/dt = \sqrt{2D}\,\boldsymbol{\eta}(t)$, where $D = k_B T/6\pi\mu a$ is the diffusivity, T is the ambient temperature, μ is the viscosity of the medium, and a is the particle radius. $\boldsymbol{\eta}$ is a white noise with zero mean, $\langle\boldsymbol{\eta}\rangle = 0$, and is delta correlated $\boldsymbol{\eta}(t)\boldsymbol{\eta}(t') = \delta(t - t')\boldsymbol{I}$, with $\boldsymbol{I}$ being the identity tensor. The exit time τ for such a colloidal particle initially present at the center of a stationary drop is $\tau \sim R^2/D$, where R is the drop radius. Drops suspended in air seldom remain stationary and start sedimenting by their own weight. The flow field inside such a sedimenting drop (Fig. 3) is given by the Hadamard-Rybczynski equation. The nondimensional stream functions describing the flow interior (ψ) and exterior ($\widehat{\psi}$) to the drop can be found in Leal [21],

$$\psi = -\frac{\sin^2\theta}{4}\frac{r^2 - r^4}{\lambda + 1}, \tag{1}$$

$$\widehat{\psi} = \frac{\sin^2\theta}{2}\left\{r^2 - \frac{3\lambda + 2}{2(\lambda + 1)} + \frac{\lambda}{2(\lambda + 1)}\frac{1}{r}\right\}. \tag{2}$$

Here, r denotes the radial distance from the drop center, nondimensionalized by the drop radius R, while θ represents the polar angle measured relative to the direction of the drop's motion. The exit time of a colloidal particle is governed by the interior flow field, which can be expressed as

$$\boldsymbol{u}(\boldsymbol{x}) = \frac{\boldsymbol{U}}{2(1 + \lambda)} \cdot [(2r^2 - 1)\boldsymbol{I} - \boldsymbol{xx}]. \tag{3}$$

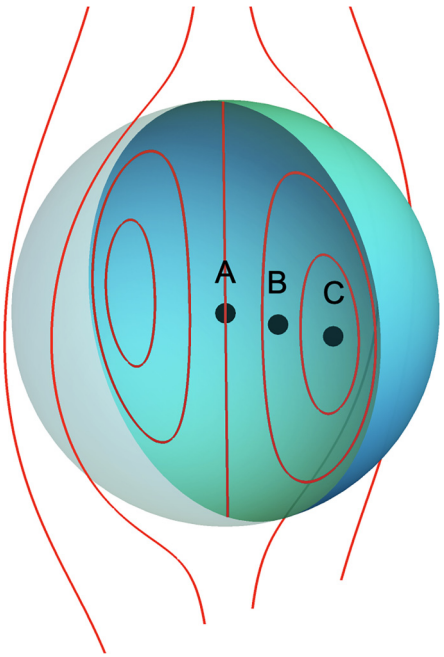

FIG. 3. The Hadamard-Rybczynski flow field inside a sedimenting drop. Points A, B, and C correspond to locations (0,0,0), (0.25,0.25,0), and (0.5,0.5,0), with all lengths in the system being scaled with the drop radius R.

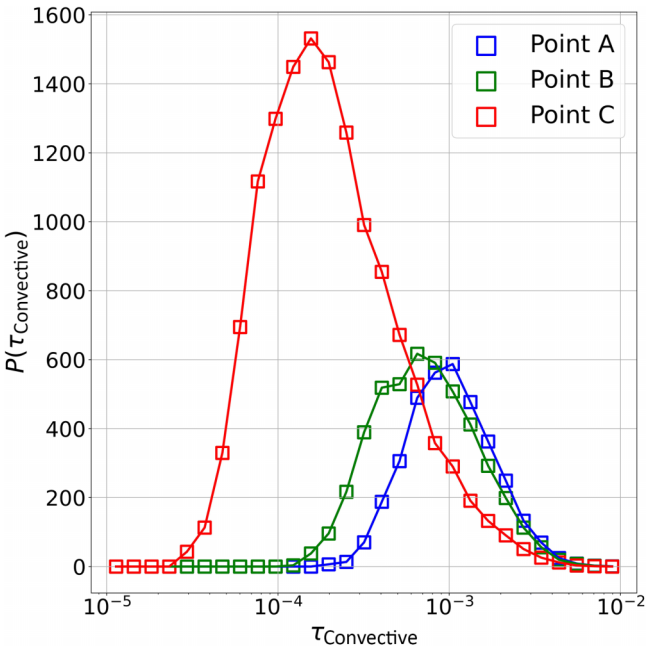

FIG. 4. Distribution of exit times from 10 000 independent Brownian dynamics realizations for particles initially located at points A, B, and C for Pe = 0.01.

$\boldsymbol{U}$ is the terminal velocity attained by the freely falling drop as given by the Hadamard-Rybczynski equation,

$$\boldsymbol{U} = \frac{2}{3}\frac{\Delta\rho g R^2}{\mu}\left(\frac{1+\lambda}{2+3\lambda}\right)\widehat{z}, \tag{4}$$

where $\Delta\rho = \rho - \widehat{\rho}$ is the density difference between the drop and the ambient fluid and g is the acceleration due to gravity. To explore the role of convection in altering the exit time of the particle, we start by performing Brownian dynamics simulations. The colloidal particle is thus forced by both the thermal fluctuations in the system as well as the Hadamard-Rybczynski velocity field seen inside a sedimenting drop,

$$\frac{d\boldsymbol{x}}{dt} = \frac{\boldsymbol{U}}{2(1+\lambda)} \cdot [(2r^2-1)\boldsymbol{I} - \boldsymbol{xx}] + \sqrt{2D}\,\boldsymbol{\eta}(t). \tag{5}$$

The above equation is nondimensionalized by scaling all lengths in the system with the drop radius R and the time t with the convective timescale $R\bar{U}$, where $\bar{U} = |\boldsymbol{U}|$ is the terminal velocity of the sedimenting drop as given in Eq. (4). This exercise yields a Péclet number $\mathrm{Pe} = \bar{U}R/(2D(1+\lambda))$, which characterizes the relative strengths of convective and diffusive transport in the system.

In the context of aerosols, a droplet of radius $R \sim 10$ μm has a terminal velocity of $\bar{U} \sim 10\ \mathrm{mm\,s^{-1}}$. This yields $\mathrm{Pe} \sim 243$ for a pathogen of radius 50 nm present inside the drop. The nondimensional form of Eq. (5) is given as

$$\frac{d\boldsymbol{x}}{dt} = \mathrm{Pe}\widehat{\boldsymbol{z}} \cdot [(2r^2-1)\boldsymbol{I} - \boldsymbol{xx}] + \sqrt{2}\,\boldsymbol{\eta}(t). \tag{6}$$

Equation (6) is solved using an Euler-Maruyama time marching scheme with a time step chosen as

$$\Delta t = 10^{-1} \times \min\left(\epsilon, \frac{\epsilon^2 \mathrm{Pe}}{2}\right). \tag{7}$$

This choice ensures that the particle displacement due to convective effects and the mean-squared displacement due to diffusive effects remain smaller than ϵ. In the simulations we choose $\epsilon = 10^{-2}$. For particles initially located at points A, B, and C within the drop (as shown in Fig. 3), the ensemble-averaged numerical solution of Eq. (6) provides the corresponding escape times as functions of Pe. The Brownian dynamics simulations were conducted over 10 000 independent realizations, and the resulting distribution of exit times from these simulations is presented in Fig. 4. The escape time varies with the initial location of the particle inside the drop (Fig. 5). Thus, the mass transport in the system is better depicted through the calculation of a mean escape time of a particle present inside a drop, for a given value of Pe. Brownian dynamics simulations are computationally intensive, rendering the evaluation of τ at a sufficiently dense set of points within the drop a costly and time-consuming process. Furthermore, the time stepping used in the numerical solution of Eq. (6) is required to be smaller than both the diffusive and the convective timescales in the system. This results in the calculation of τ for $\mathrm{Pe} \gg 1$ to be computationally more expensive. In the next section of the paper, we calculate the mean exit time through a probabilistic formulation of τ.

III. THE BACKWARD KOLMOGOROV EQUATION

The probabilistic formulation invokes the definition of a transition probability $\mathcal{F}(\boldsymbol{x}, t\,|\,\boldsymbol{x_0}, t_0)$, which represents the

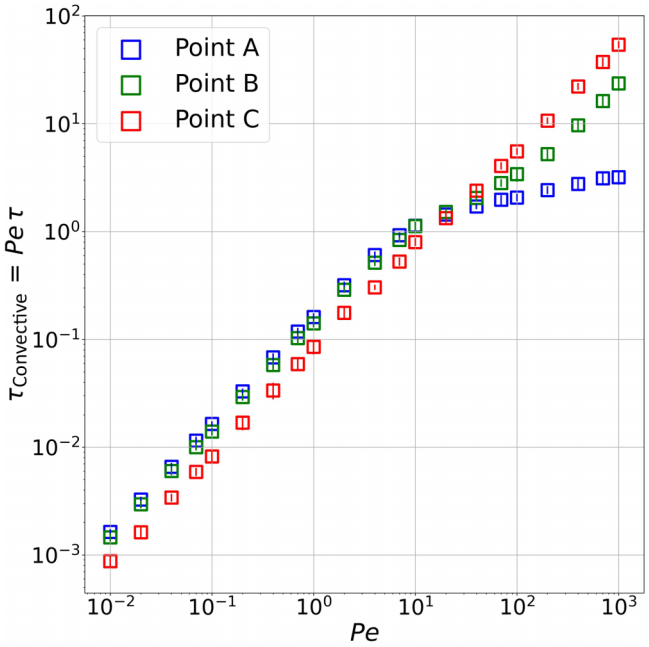

FIG. 5. The escape time τ is computed for particles starting from points A (0,0,0), B (0.25,0.25,0), and C (0.5,0.5,0), as indicated in Fig. 3, across a range of Péclet numbers (Pe). The vertical lines represent the standard deviation obtained from ensemble averaging over 10 000 realizations for each data point.

probability distribution function associated with finding a particle at the location $\boldsymbol{x}$ at time t, given that it was present at $\boldsymbol{x_0}$ at time t_0. Such a transition probability distribution is governed by a forward Kolmogorov equation (also known as a Fokker-Planck equation) as follows:

$$\frac{\partial \mathcal{F}}{\partial t} + \nabla \cdot (\boldsymbol{u}\mathcal{F} - D\nabla\mathcal{F}) = 0. \tag{8}$$

The boundary conditions for Eq. (8) consist of the distribution function going to zero at a free boundary (Ω_e), which allows for a free exit of the particle, and a no-flux condition at the walls of the boundary (Ω_w):

$$\mathcal{F} = 0 \quad \forall \boldsymbol{x} \in \Omega_e, \tag{9a}$$

$$\widehat{\boldsymbol{n}} \cdot \big(\boldsymbol{u} - D\nabla\big)\mathcal{F} = 0 \quad \forall \boldsymbol{x} \in \Omega_w, \tag{9b}$$

where $\widehat{n}$ denotes the normal to the wall boundary Ω_w. Integrating $\mathcal{F}(\boldsymbol{x}, t, |, \boldsymbol{x}_0, t_0)$ over the entire domain gives a quantity known as the survival probability,

$$S(t\,|\,\boldsymbol{x}_0, t_0) = \int_{\Omega} \mathcal{F}(\boldsymbol{x}, t\,|\,\boldsymbol{x}_0, t_0) dV, \tag{10}$$

which depicts the distribution function of finding a particle anywhere in the domain at time t given that it was initially at location $\boldsymbol{x}_0$ at time t_0. The quantity $-\partial S/\partial t$ pertains to the first-passage distribution function for a particle at time t. The exit time for a particle inside the domain can be written as the following weighted average:

$$\tau(\boldsymbol{x}_0, t_0) = -\int_{t_0}^{\infty} (t - t_0)\frac{\partial S}{\partial t} dt. \tag{11}$$

Through the use of the Chapman-Kolmogorov equation, it can be shown that $\mathcal{F}$ also obeys the backward Kolmogorov equation (see Thiffeault [17] Appendix 2.A),

$$-\frac{\partial \mathcal{F}}{\partial t_0} - \nabla_{\boldsymbol{x}_0} \cdot (\boldsymbol{u}\mathcal{F} + D\nabla_{\boldsymbol{x}_0}\mathcal{F}) = 0. \tag{12}$$

Using Eqs. (10)–(12), it can be shown that the exit time formulated as a first-passage process is governed by the following backward Kolmogorov equation (Redner [1] and Thiffeault [17]):

$$\mathrm{Pe}\,\boldsymbol{u} \cdot \nabla_{\boldsymbol{x}_0}\tau + \nabla^2_{\boldsymbol{x}_0}\tau + 1 = 0. \tag{13a}$$

In the above equation, all lengths have been scaled with the drop radius R, and t has been scaled using the diffusive timescale (R^2/D). A Dirichlet boundary condition is imposed at the drop boundary since the exit time for a particle at the boundary is zero.

$$\tau = 0 \quad \forall \boldsymbol{x} \in \Omega_S, \tag{13b}$$

where Ω_S represents the drop boundary. Due to the drop's spherical nature, it is convenient to write Eq. (13a) in spherical polar coordinates,

$$\mathrm{Pe}\left[u_r\frac{\partial \tau}{\partial r} + \frac{u_\theta}{r}\frac{\partial \tau}{\partial \theta}\right] + \frac{1}{r^2}\frac{\partial}{\partial r}\left\{r^2\frac{\partial \tau}{\partial r}\right\} + \frac{1}{r^2\sin\theta}\frac{\partial}{\partial \theta}\left\{\sin\theta\frac{\partial \tau}{\partial \theta}\right\} + 1 = 0, \tag{14}$$

with (13b) transforming to

$$\tau = 0 \text{ at } r = 1, \tag{15a}$$

$$\tau \text{ is bounded at } r = 0. \tag{15b}$$

The flow velocity in spherical polar coordinates is given by [13]

$$u_r = (1 - r^2)\cos\theta, \quad u_\theta = (2r^2 - 1)\sin\theta. \tag{16}$$

For a given value of Pe, Eq. (14) can be solved numerically to determine τ, and the mean exit time can then be estimated by averaging τ over all spatial positions within the domain.

A. Diffusion-dominated regime (Pe ≪ 1)

In the diffusion-dominated regime of Pe $\ll 1$, it is possible to arrive at an analytical expression for the exit time through a perturbation expansion of τ,

$$\tau = \tau_0 + \mathrm{Pe}\tau_1 + \mathrm{Pe}^2\tau_2 + O(\mathrm{Pe}^3). \tag{17}$$

At leading order, the governing equation for τ_0 reduces to a purely diffusive and hence isotropic problem with boundary conditions that do not depend on θ. By symmetry and uniqueness, τ_0 is therefore a function of r alone, $\tau_0 = \tau_0(r)$. The perturbation expansion from Eq. (17) applied to Eq. (14) yields the following results at $O(1)$:

$$\frac{1}{r^2}\frac{\partial}{\partial r}\left\{r^2\frac{\partial \tau_0}{\partial r}\right\} + 1 = 0 \Rightarrow \tau_0 = \frac{1}{6}(1 - r^2). \tag{18}$$

At $O(\mathrm{Pe})$,

$$-\frac{1}{3}(1-r^2)r\cos\theta+\frac{1}{r^2}\frac{\partial}{\partial r}\left\{r^2\frac{\partial\tau_1}{\partial r}\right\}+\frac{1}{r^2\sin\theta}\frac{\partial}{\partial\theta}\left\{\sin\theta\frac{\partial\tau_1}{\partial r}\right\}=0$$

$$\Rightarrow \tau_1=\frac{1}{420}\left\{-9r+14r^3-5r^5\right\}\cos\theta. \tag{19}$$

At $O(\mathrm{Pe}^2)$,

$$(1-r^2)\cos^2\theta\frac{\partial\tau_1}{\partial r}+\frac{1}{r}(2r^2-1)\sin\theta\frac{\partial\tau_1}{\partial\theta}+\frac{1}{r^2}\frac{\partial}{\partial r}\left\{r^2\frac{\partial\tau_2}{\partial r}\right\}+\frac{1}{r^2\sin\theta}\frac{\partial}{\partial\theta}\left\{\sin\theta\frac{\partial\tau_2}{\partial r}\right\}=0$$

$$\Rightarrow \tau_2=\mathcal{F}_1+\mathcal{F}_1P_2(\cos\theta), \tag{20}$$

where

$$\mathcal{F}_1=\frac{(r^2-1)^3(31-5r^2)}{30\,240}\quad\text{and}$$

$$\mathcal{F}_2=-\frac{(r^2-1)r^2(315r^4-994r^2+887)}{873\,180}.$$

The accuracy of the asymptotic predictions is demonstrated by comparison with Brownian dynamics simulations, as shown in Fig. 6. The asymptotic results exhibit good agreement for $\mathrm{Pe}\lesssim 10$, beyond which they fail to capture the escape time in the convection-dominated regime. The solution from Eqs. (18)–(20) allows for a spatial averaging of the exit time over the entire drop and the calculation of a mean exit time $\langle\langle\tau\rangle\rangle$,

$$\langle\langle\tau\rangle\rangle=\tfrac{1}{15}-\tfrac{148}{1\,091\,475}\mathrm{Pe}^2+O(\mathrm{Pe}^3). \tag{21}$$

In computing the mean exit time, we assume that the particle's initial position within the drop is uniformly distributed. While the exit time for an individual particle, as derived in Eqs. (17)–(20), includes a correction at $O(\mathrm{Pe})$, the mean exit time given by Eq. (21) is shown to be an even function of Pe. The lack of an $O(\mathrm{Pe})$ correction in the mean exit time arises from the fore-aft symmetry about the drop center displayed by the internal velocity field, which corresponds to the classical Hadamard-Rybczynski solution. Because of this symmetry, the $\mathcal{O}(\mathrm{Pe})$ correction contains equal and oppositely signed contributions from pairs of symmetric points, which cancel upon spatial averaging. As a result, the leading nonzero correction appears at $O(\mathrm{Pe}^2)$, and the mean exit time becomes an even function of Pe. Physically, this implies that $\langle\langle\tau\rangle\rangle$ depends only on the magnitude of the translational velocity and not on its direction.

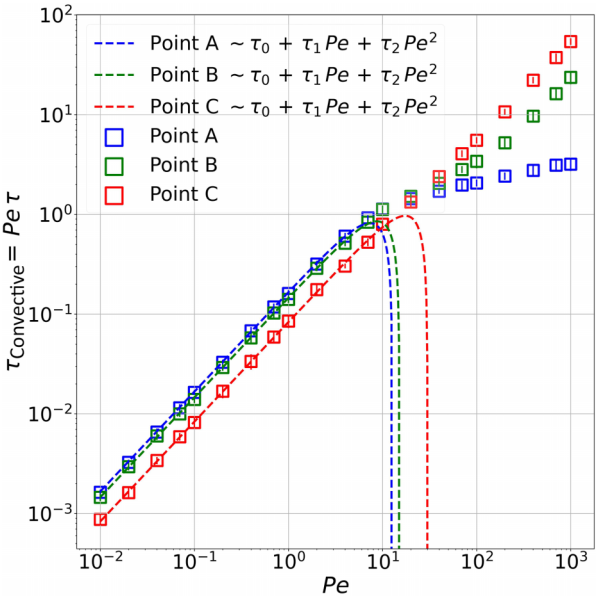

FIG. 6. A comparison of the Brownian dynamics simulations [Eq. (6)] and the $\mathrm{Pe}\ll 1$ asymptotics [Eqs. (18)–(20)] for a particle starting from points A (0,0,0), B (0.25,0.25,0), and C (0.5,0.5,0) as indicated in Fig. 3, across various values of Pe.

B. Convection-dominated regime ($\mathrm{Pe}\gg 1$)

In the limit of $\mathrm{Pe}\gg 1$, due to the convective timescale being much smaller than the diffusive timescale, the backward Kolmogorov equation is written down using a convective timescaling as follows:

$$\frac{1}{\mathrm{Pe}}\left[\frac{1}{r^2}\frac{\partial}{\partial r}\left\{r^2\frac{\partial\tau_c}{\partial r}\right\}+\frac{1}{r^2\sin\theta}\frac{\partial}{\partial\theta}\left\{\sin\theta\frac{\partial\tau_c}{\partial\theta}\right\}\right]+\left[u_r\frac{\partial\tau_c}{\partial r}+\frac{u_\theta}{r}\frac{\partial\tau_c}{\partial\theta}\right]+1=0, \tag{22}$$

where $\tau_c=\mathrm{Pe}\tau$ is the exit time based on a convective timescale. For $\mathrm{Pe}\gg 1$, the diffusive flux can be ignored and Eq. (22) becomes

$$\left[u_r\frac{\partial\tau_c}{\partial r}+\frac{u_\theta}{r}\frac{\partial\tau_c}{\partial\theta}\right]+1=0. \tag{23}$$

Following the work of Kronig and Brink [3], it is possible to shift to a coordinate system based on the flow streamlines (with stream function ψ) within the drop,

$$\tau(r,\theta)\equiv\tau(\xi),$$

$$\text{where } \xi=16(1+\lambda)\psi=4r^2(1-r^2)\sin^2\theta. \tag{24}$$

This transformation to the streamline coordinates is enabled by the fact that the variation of the particle concentration remains negligibly small along a flow streamline due to the strong effects of convective transport. The transport enabled through the thermal fluctuations in the system exists only through the cross-streamline diffusive flux (see Kronig and

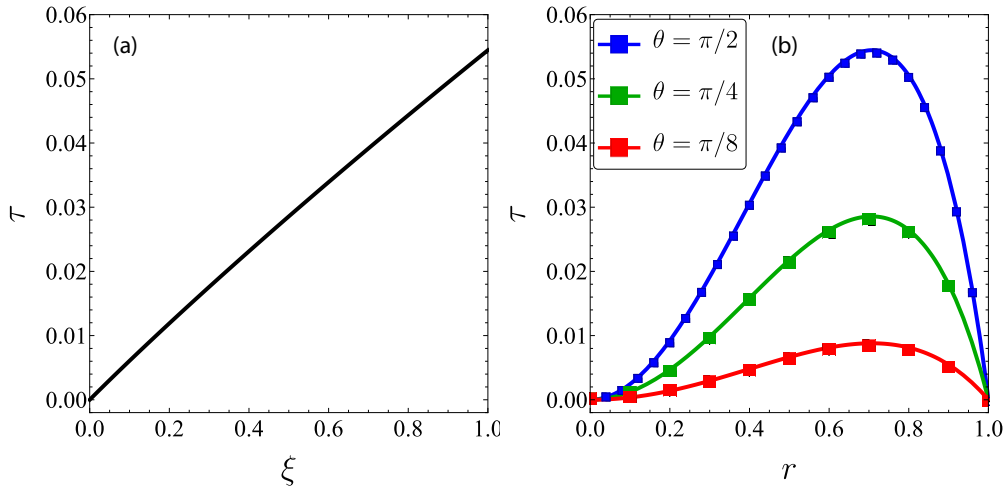

FIG. 7. (a) The numerical solution for $\tau(\xi)$ given by (25) and (b) the exit time τ for varying r for $\theta = \pi/2, \pi/4$, and $\pi/8$ calculated from Eq. (25) (indicated by solid lines) and from the full numerical solution of the backward Kolmogorov equation given by Eq. (14) (indicated by the dots and discussed further in Sec. III C).

Brink [3] and Yu-Fang and Acrivos [5]). Thus, Eq. (23) transforms as

$$\frac{\partial}{\partial\xi}\left(\mathcal{A}(\xi)\frac{\partial\tau}{\partial\xi}\right) = \frac{\mathcal{B}(\xi)}{16}, \tag{25}$$

$$\text{where } \mathcal{B}(\xi) = \frac{2}{\sqrt{1+\sqrt{\xi}}}K\left(\frac{1-\sqrt{\xi}}{1+\sqrt{\xi}}\right),$$

$$\mathcal{A}(\xi) = \frac{2\sqrt{1+\sqrt{\xi}}}{3}\left[(4-3\xi)E\left(\frac{1-\sqrt{\xi}}{1+\sqrt{\xi}}\right)\right.$$

$$\left. - (4\sqrt{\xi}-3\xi)K\left(\frac{1-\sqrt{\xi}}{1+\sqrt{\xi}}\right)\right]. \tag{26}$$

Here, the functions K and E denote the complete elliptic integrals of the first and second kind, respectively. These elliptic integrals are evaluated using standard numerical routines. The boundary conditions from (15a) are modified as

$$\tau = 0 \text{ at } \xi = 0, \tag{27a}$$

$$\tau \text{ is bounded at } \xi = 1. \tag{27b}$$

The above system is solved numerically to obtain the exit time as a function of the streamline coordinate ξ [see Fig. 7(a)]. The exit time exhibits a maximum near $\xi \approx 1$. For $\theta = \pi/2$, this corresponds to τ attaining its peak value at $r = 1/\sqrt{2}$ [Fig. 7(b)], which coincides with the location of the vortex center in the Hadamard-Rybczynski flow field. The mean exit time $\langle\langle\tau_c\rangle\rangle$ can be calculated using a spatial averaging given as follows (see Kronig and Brink [3]):

$$\langle\langle\tau\rangle\rangle = \frac{3}{8}\int_0^1 \tau(\xi)\mathcal{B}(\xi)d\xi, \tag{28}$$

which yields $\langle\langle\tau\rangle\rangle = 0.0258$ for the asymptote $\mathrm{Pe} \gg 1$.

C. Numerical solution of backward Kolmogorov equation

A better picture of the exit time $\tau(r,\theta)$ for arbitrary values of Pe is possible through the numerical solution of Eq. (22). A comparison of the full numerical solution with the $\mathrm{Pe} \ll 1$ and $\mathrm{Pe} \gg 1$ asymptotics along with the results from the Brownian dynamics simulations is shown in Fig. 8. The numerical solver is employed to compute the contours of exit time for a given value of Pe. It can be observed from Figs. 9(a) and 9(b) that at low values of Pe the exit-time contours are fairly isotropic due to the low strength of convection in the system. At a larger value of $\mathrm{Pe} = 1000$ [Fig. 9(d)], the exit-time contours closely resemble the Hadamard-Rybczynski flow field shown in Fig. 3. The numerical solution allows for a more robust calculation of the mean exit time described by Eq. (28).

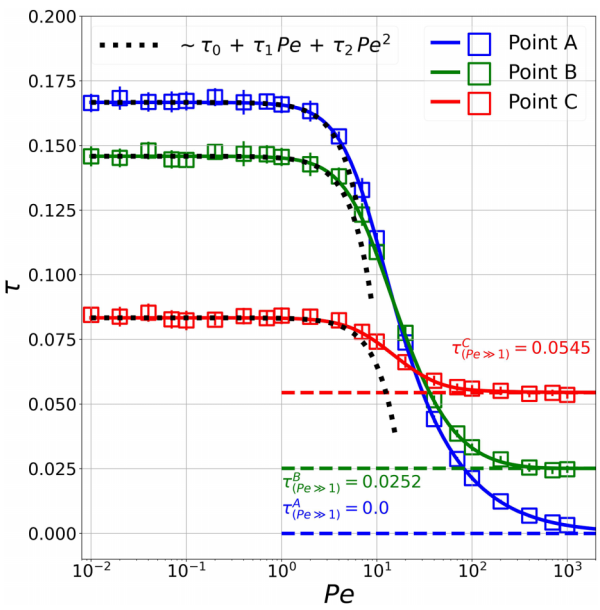

FIG. 8. The escape time τ with varying Pe for a particle starting from points A (0,0,0) (blue), B (0.25,0.25,0) (green), and C (0.5,0.5,0) (red) as displayed in Fig. 3. The solid lines pertain to the full numerical solution of Eq. (22) for a particle starting from points A, B, and C. The open squares correspond to the exit times from the Brownian dynamics calculations. The colored dashed lines pertain to the limit of $\mathrm{Pe} \gg 1$ and the dotted black lines pertain to the asymptotic solution for the $\mathrm{Pe} \ll 1$ limit derived in Eqs. (18)–(20).

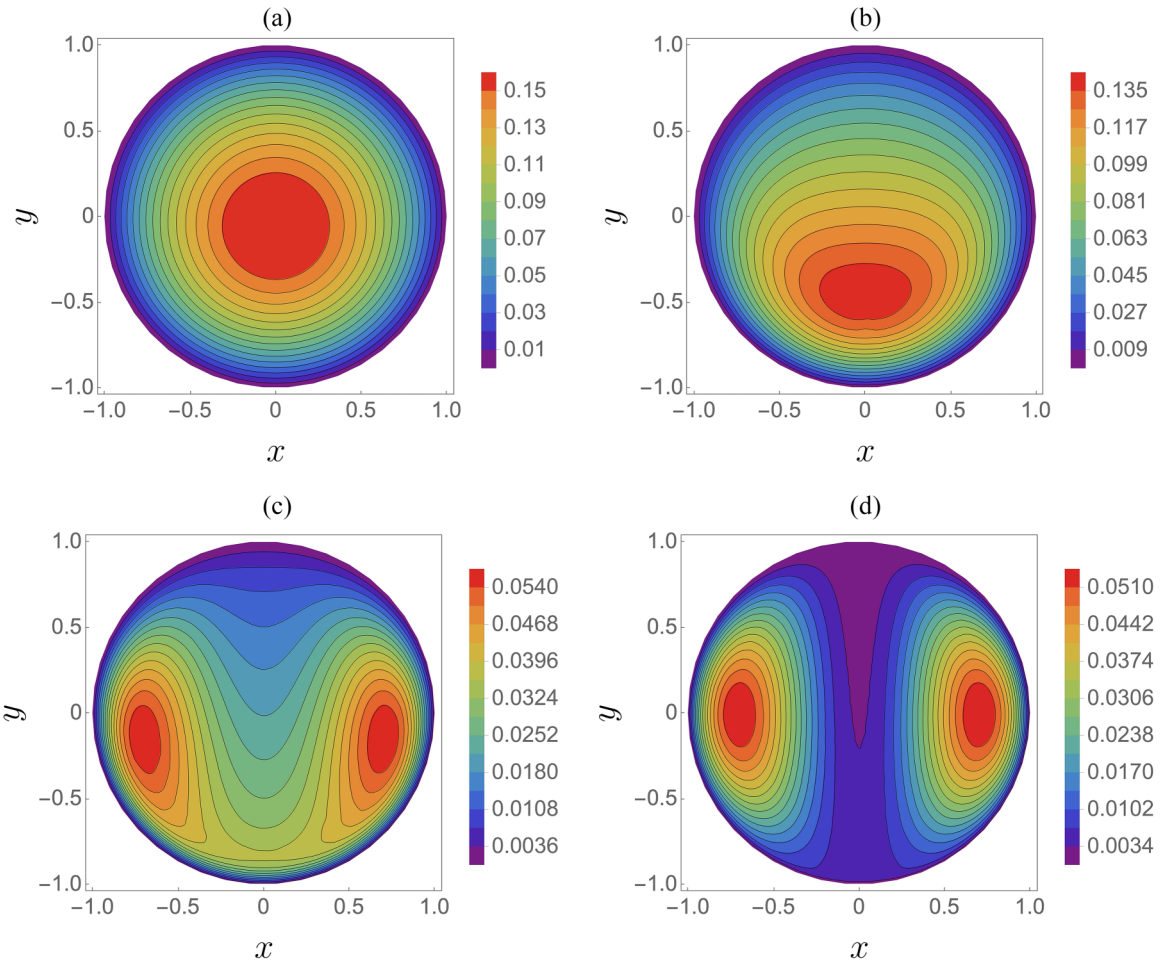

FIG. 9. The contour plots depicting the exit time τ for (a) Pe = 1, (b) Pe = 10, (c) Pe = 100, and (d) Pe = 1000.

Figure 10 gives the variation of the mean exit time $\langle\langle\tau\rangle\rangle$ across different values of Pe. The mean exit time is analogous to the bulk temperature seen from the work on heat transport in a falling drop by Kronig and Brink [3].

The mean exit time ($\langle\langle\tau\rangle\rangle$) as a function of the Péclet number (Fig. 10) has then been used to estimate the exit time of particles of varying sizes from droplets of different radii as shown in Fig. 11. For example, the mean exit time of a 10-nm-sized colloidal particle from a 20 μm drop, when driven purely by the thermal fluctuations, is approximately 1 s. In contrast, when convective transport within the sedimenting drop is taken into account, the exit time decreases to around ∼0.4 s, representing a roughly 2.5-fold speedup. These results underscore the crucial role played by the convective flow in governing the transport characteristics of the system.

IV. CONCLUSION

In this work, we introduce an exit-time-based metric for quantifying transport within droplets. This metric stands in contrast to most theoretical studies on mass transfer, which focus on long-time asymptotic diagnostics, such as Sherwood or Nusselt numbers. These quantities often characterize the

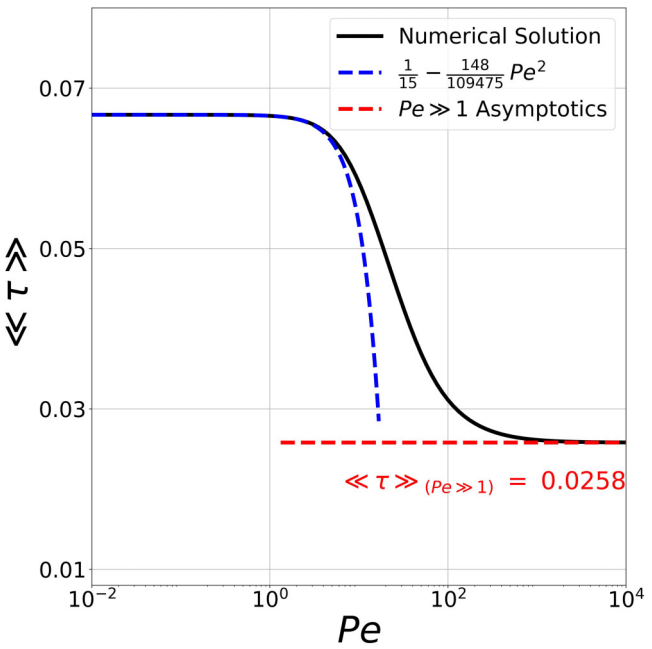

FIG. 10. The average escape time $\langle\langle\tau\rangle\rangle$ with varying Pe.

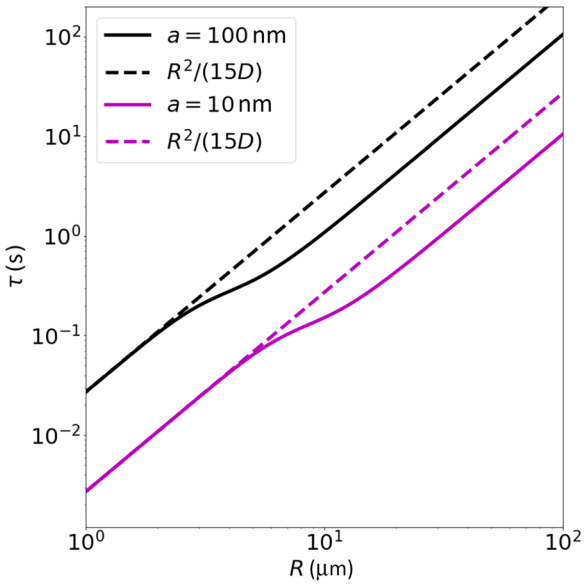

FIG. 11. The exit time in seconds for 10 and 100 nm particles present inside drops of radius R (μm).

final quasisteady or ultimate transport state, which may not be experimentally relevant, either due to limited observation times or finite droplet lifetimes. Exit time, on the other hand, is a finite-time, experimentally measurable quantity that serves as a practical and physically meaningful descriptor of solute or particle transport in realistic droplet systems.

We demonstrate that the exit-time calculation of a colloidal-sized particle can be effectively formulated as a first-passage process. By leveraging the backward Kolmogorov equation, we obtain numerical solutions that provide a computationally efficient alternative to Lagrangian simulations. The accuracy of this stochastic approach is validated by the results presented in Fig. 8, highlighting its reliability in predicting exit times. Furthermore, this method offers a scalable framework for characterizing mass transport in arbitrary flow conditions, with significantly lower computational costs compared to Brownian dynamics simulations or solving full scalar transport equations.

One particularly relevant application of this approach lies in understanding aerosol transmission of pathogenic diseases. The results from Fig. 11 reveal that larger droplets facilitate faster particle exit due to enhanced convective effects. The plot exhibits a smooth crossover from the diffusion-dominated regime, where the exit time scales as $\sim R^2/(15D)$, to the convection-dominated regime, where enhanced convective transport accelerates particle escape. Experimental validation of these predictions—such as measuring the residence time of droplets expelled during sneezing or coughing—could help identify the size ranges most conducive to airborne disease transmission. Beyond biomedical applications, this framework can also be extended to study colloidal particle dynamics inside cloud droplets. In atmospheric sciences, understanding the residence time of particles within cloud droplets is crucial for predicting their impact on cloud formation, growth, and precipitation processes. The stochastic formulation presented here could provide a computationally efficient means to model particle transport under turbulent cloud conditions, aiding in the study of cloud microphysics and aerosol-climate interactions.

While the present framework offers broad applicability, it does not account for interactions between colloidal particles and the drop interface. In particular, when the separation between the particle and the drop surface becomes small, lubrication-type interactions can give rise to secondary flows. These flows, and the associated resistance tensor, may alter the particle's exit time and potentially deform the drop interface. Future extensions of this work could incorporate these interactions to provide a more complete description. Additionally, applying the stochastic framework to chaotic fluid systems could provide new insights into finite-time transport phenomena in complex flow environments.

ACKNOWLEDGMENTS

A.R. is grateful to Prof. Jean-Luc Thiffeault for providing an introduction to exit-time problems. The authors would like to thank the DST-SERB for funding this work through a grant with Reference No. MSC/2020/000300.

DATA AVAILABILITY

The data that support the findings of this article are not publicly available upon publication because it is not technically feasible and/or the cost of preparing, depositing, and hosting the data would be prohibitive within the terms of this research project. The data are available from the authors upon reasonable request.

[1] S. Redner, *A Guide to First-Passage Processes* (Cambridge University Press, Cambridge, 2012).
[2] U. Lohmann and J. Feichter, Global indirect aerosol effects: A review, Atmos. Chem. Phys. **5**, 715 (2005).
[3] R. Kronig and J. Brink, On the theory of extraction from falling droplets, Appl. Sci. Res. **2**, 142 (1951).
[4] D. L. Oliver and A. W. Souccar, Heat transfer from a translating droplet at high peclet numbers: Revisiting the classic solution of Kronig & Brink, J. Heat Transfer **128**, 648 (2006).
[5] P. Yu-Fang and A. Acrivos, Heat transfer at high péclet number in regions of closed streamlines, Int. J. Heat Mass Transfer **11**, 439 (1968).
[6] J. F. Lingevitch and A. J. Bernoff, Advection of a passive scalar by a vortex couple in the small-diffusion limit, J. Fluid Mech. **270**, 219 (1994).
[7] R. Griffiths, Particle motions induced by spherical convective elements in stokes flow, J. Fluid Mech. **166**, 139 (1986).
[8] J. Turner, The flow into an expanding spherical vortex, J. Fluid Mech. **18**, 195 (1964).

[9] S. Jana and J. Ottino, Chaos-enhanced transport in cellular flows, Philos. Trans. R. Soc. Lond. Ser. A **338**, 519 (1992).
[10] K. Bajer and H. Moffatt, On a class of steady confined stokes flows with chaotic streamlines, J. Fluid Mech. **212**, 337 (1990).
[11] H. Stone, A. Nadim, and S. H. Strogatz, Chaotic streamlines inside drops immersed in steady stokes flows, J. Fluid Mech. **232**, 629 (1991).
[12] M. D. Bryden and H. Brenner, Effect of laminar chaos on reaction and dispersion in eccentric annular flow, J. Fluid Mech. **325**, 219 (1996).
[13] D. Kroujiline and H. Stone, Chaotic streamlines in steady bounded three-dimensional stokes flows, Phys. D (Amsterdam, Neth.) **130**, 105 (1999).
[14] C. Christov and G. Homsy, Enhancement of transport from drops by steady and modulated electric fields, Phys. Fluids **21**, 083102 (2009).
[15] D. Krishnamurthy and G. Subramanian, Heat or mass transport from drops in shearing flows. Part 1. The open streamline regime, J. Fluid Mech. **850**, 439 (2018).
[16] G. Batchelor and J. Nitsche, Expulsion of particles from a buoyant blob in a fluidized bed, J. Fluid Mech. **278**, 63 (1994).
[17] J.-L. Thiffeault, Exit time problems for swimming microorganisms, 2018, https://people.math.wisc.edu/~thiffeault/lecturing/exit-minicourse/exit-minicourse.pdf.
[18] F. Marcotte, C. R. Doering, J.-L. Thiffeault, and W. R. Young, Optimal heat transfer and optimal exit times, SIAM J. Appl. Math. **78**, 591 (2018).
[19] L. Morawska, G. R. Johnson, Z. D. Ristovski, M. Hargreaves, K. Mengersen, S. Corbett, C. Y. H. Chao, Y. Li, and D. Katoshevski, Size distribution and sites of origin of droplets expelled from the human respiratory tract during expiratory activities, J. Aerosol Sci. **40**, 256 (2009).
[20] A. Souccar and D. L. Oliver, Transfer from a droplet at high peclet numbers with heat generation: Interior problem, J. Heat. Transfer **129**, 664 (2007).
[21] L. G. Leal, *Advanced Transport Phenomena: Fluid Mechanics and Convective Transport Processes* (Cambridge University Press, Cambridge, 2007), Vol. 7.